Available online at www.sciencedirect.com
ScienceDirect
Journal of Power Sources 162 (2006) 436–443
JOURNAL OF POWER SOURCES
www.elsevier.com/locate/jpowsour

Measurement of the interface adhesion of solid oxide fuel cells by indentation

Yongsong Xie*, Xinge Zhang, Mark Robertson, Radenka Maric, Dave Ghosh

Institute for Fuel Cell Innovation, National Research Council Canada, 4250 Wesbrook Mall, Vancouver, BC, Canada V6T 1W5

Received 27 June 2006; received in revised form 14 July 2006; accepted 14 July 2006
Available online 1 September 2006

Abstract

The adhesion between two adjacent layers in a solid oxide fuel cell (SOFC) is critically important to ensure the desired performance. However, measuring the interface adhesion is very difficult because most layers in an SOFC are brittle and/or porous. This paper introduces a simple technique for the quantitative measurement of interface adhesion of SOFCs. A hard, spherically tipped indenter is driven through the top layer(s) and into the underlying substrate of a plate SOFC specimen. Extensive plastic deformation of the substrate causes an interface annular crack. The interface adhesion is then calculated from the radius of the annular crack. The indentation method should be suitable for the adhesion measurement of any SOFC with a porous support. A measurement procedure and the related calculation equations for determining the interface adhesion are presented in this paper. The interface adhesion of a cermet-supported SOFC with a doped ceria electrolyte for operation at 400–600 °C was measured to demonstrate the use of the indentation method. The measurement indicated that the cermet-supported SOFC had sufficient interface adhesion.

Keywords: Solid oxide fuel cell; Adhesion measurement; Indentation; Interface adhesion; Interface toughness

1. Introduction

A solid oxide fuel cell (SOFC) is a device that converts the chemical energy of fuels electrochemically to electricity. It is essentially a ceramic device consisting of a dense electrolyte sandwiched between a porous fuel electrode (anode) and a porous air electrode (cathode). SOFCs can be divided into anode-supported, electrolyte-supported, cathode-supported and substrate-supported [1]. In the latter, the substrate can be either a porous metal or a porous cermet [2,3].

To ensure adequate performance, three requirements are necessary for adjacent layers in an SOFC: sufficient adhesion, well-adjusted chemical compatibility and well-matched thermal expansion behavior. Although it is of practical importance to measure the interface adhesion of an SOFC, no standard method for such measurement is available. SOFC researchers can only use inaccurate methods to estimate the adhesion between two adjacent layers. For example, a scalpel was used to assess anode-electrolyte adhesion by gently scratching the anode layer. Then, adhesion was determined to be sufficient when the layer remained attached to the electrolyte after the scratch [4].

Several methods exist for measuring the adhesion of a ceramic coating to the underlying substrate. In the pull-off method [5], the most widely used, a loading bar is bonded to the top surface of a coating with an adhesive bonding agent. Then a force normal to the coating–substrate interface is applied to determine the critical force for coating detachment. However, it may be challenging to apply this method to SOFCs because (1) it is difficult to prevent the penetration of the adhesive bonding agent from porous electrode layer into the interface of which the adhesion strength should be measured, and (2) the interface adhesion strength that can be measured by this method is limited by the adhesion strength of the bonding agent, which is usually less than 80 MPa [e.g. 6], a value lower than that of many interfaces in SOFCs.

The four-point bending method measures interface toughness by pre-cracking a coated beam specimen and then monitoring the onset of delamination with increasing bending load [7]. Measuring the interface toughness via this method, however, is restricted to coating–substrate combinations, wherein the frac-

* Corresponding author. Tel.: +1 604 221 3074; fax: +1 604 221 3001.
E-mail address: yongsong.xie@nrc.gc.ca (Y. Xie).

0378-7753/$ – see front matter © 2006 Elsevier B.V. All rights reserved.
doi:10.1016/j.jpowsour.2006.07.034

ture toughness of the coating is relatively high to prevent the coating from vertical cracking. Vertical cracking, and thus segmentation, decreases the stored elastic energy in the coating and makes the accurate measurement of the interface fracture energy impossible. By bonding an additional metallic stiffening layer to the top surface of a coating, the four-point bending method was modified to measure the interface adhesion of thin, brittle layers tending to separate by vertical cracks [8]. However, as in the pull-off method, the modified four-point bending method is not applicable to SOFCs due to the likely penetration of the bonding agent into the interface from the porous electrode layer.

In the scratch adhesion test, a popular method for assessing the adhesion of a thin coating to a relatively soft substrate, a spherically tipped diamond indenter is drawn along the coated surface. The normal load applied to the indenter is increased continuously or stepwise until a critical load is reached. At the critical normal load, the radial compressive stress over a certain area ahead of the indenter exceeds the critical value needed to drive the delamination of the coating [9]. This critical normal load is usually measured by using an acoustic emission detector to detect the elastic energy released from the interface fracture. The measured critical load is then taken as a semi-quantitative measure of the coating–substrate adhesion because there is no mathematic equation available to correlate the critical normal load to the interface adhesion. When applying the scratch adhesion test to brittle substrate-brittle coating systems, such as many SOFCs, a load sufficiently high to cause coating delamination is very likely to cause substrate cracking too. The substrate cracking results in specimen rupture, or, causes an additional acoustic emission signal. This additional signal makes it difficult to distinguish the signal from the coating delamination; thus, the critical load for the coating delamination is difficult to be measured in such a brittle substrate-brittle coating system.

In the indentation method, the simplest one, coating delamination is obtained by penetration of the coating with a rigid indenter. The indenter induces a compressive radial stress in the coating. This compressive stress provides the driving force for coating delamination. In some tests, the indenter only induces significant plastic deformation in the coating [e.g. 10], while in others it produces significant plastic deformation in the substrate as well [e.g. 11]. The former test is only suitable for measuring coatings with poor adhesion strength.

In the indentation method involving significant plastic deformation in the substrate, a hard indenter, either an axisymmetric indenter [11] or a wedge indenter [12], penetrates through a coating and into the underlying substrate to cause coating delamination. As schematically illustrated in Fig. 1, when a hard, axisymmetric indenter is forced through a coating and into the underlying substrate, severe plastic deformation of the substrate takes place to accommodate the indenter. The severe plastic deformation forces the coating to be displaced radially, thus, induces a compressive radial stress in the coating that decreases with increasing distance from the indent. The indenter creates a free edge in the coating at the radius $r = a$ where the indenter contacts the coating. From this edge, where the coating experiences the highest induced stresses, an interface annular crack between the coating and the substrate is initiated when the indentation-induced stresses are sufficiently high. Then, at a higher indentation load, the interface crack spreads outward radially to release the elastic strain energy stored in the coating until the point $r = R$ where the energy release rate available to drive the interface cracking drops below the interface adhesion.

The indentation testing involving significant plastic deformation in the substrate has been successfully used for quantitatively measuring the adhesion of a brittle coating on a ductile substrate [11–13]. However, this method has not been used for measuring the adhesion of a coating on a brittle substrate because a brittle substrate tends to rupture in the testing where a high load has to be applied to cause significant plastic deformation in the substrate. When a hard and sharp indenter indents a brittle specimen at a high load, propagating macro cracking is very likely to develop in the specimen. However, if the hard indenter has a blunt tip and the indented specimen is porous or heterogeneous (even if the specimen is made of a brittle material such as a ceramic), propagating macro cracking cannot develop because the stresses induced by a blunt indenter are not very intense and the porous or heterogeneous microstructure deflects the propagation of any macro cracks. This behavior allows quasi-plastic deformation to occur in the specimen [14]. Because most SOFCs are supported by porous structure components, the indentation method using a hard, spherical tipped indenter should be applicable to the measurement of the adhesion between two adjacent layers in these SOFCs. The purpose of this paper, therefore, is to demonstrate that, using a measurement procedure developed by the authors, the interface adhesion of an SOFC which has a porous support can be measured by the indentation method.

2. Theoretical solutions

As shown in Fig. 1, in the indentation made by an axisymmetric indenter, the indentation-induced interface annular crack spreads outward radially to the point $r = R$. Using appropriate equations of fracture mechanics, the interface adhesion can be calculated from the indent radius a, the radius of interface crack R, the coating thickness and the mechanical properties of the coating and the substrate.

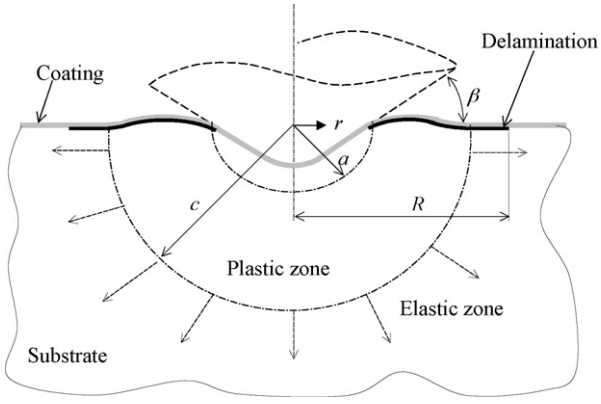

Fig. 1. Schematic of delamination induced by an axisymmetric indentation.

During the indentation, the indentation-induced interface crack spreads outward radially to release the elastic strain energy stored in the coating. The energy release rate G at the crack front, which has a radius $r = R$, is given by [11]

$$G = \frac{(1-\nu_c^2)h}{2E_c}[\sigma_r(R) - \sigma_r(R^-)]^2 \quad (1)$$

where ν_c, E_c and h are the Poisson's ratio, Young's modulus and thickness of the coating, and $\sigma_r(R)$ and $\sigma_r(R^-)$ are, respectively, the radial stress components of the coating just outside the crack front (un-delaminated edge) and just inside the crack front (delaminated edge) of the annular plate. The value of $\sigma_r(R) - \sigma_r(R^-)$, the jump in radial stress component of the coating, is the driven force for the interface cracking.

Since the elastic strain energy released from the coating is consumed by debonding the coating, the interface toughness Γ_c, which is a measure of the interface adhesion, is thus equal to the energy release rate value by

$$\Gamma_c = G = \frac{(1-\nu_c^2)h}{2E_c}[\sigma_r(R) - \sigma_r(R^-)]^2 \quad (2)$$

The radial stress component at the un-delaminated edge, $\sigma_r(R)$, is given by the generalized Hook's law

$$\sigma_r(R) = \frac{E_c}{1-\nu_c^2}[\varepsilon_r(R) + \nu\varepsilon_\theta(R)] \quad (3)$$

where ε_r and ε_θ are the radial and circumferential surface strains which are the sums of the indentation-induced radial and circumferential stains, ε_{ir} and $\varepsilon_{i\theta}$, and the initial residual strain in the coating ε_0 by the equations

$$\varepsilon_r = \varepsilon_{ir} + \varepsilon_0 \quad (4)$$

and

$$\varepsilon_\theta = \varepsilon_{i\theta} + \varepsilon_0 \quad (5)$$

ε_0 is determined by the initial residual stress of the coating, σ_0, by the equation

$$\varepsilon_0 = \frac{1-\nu_c}{E_c}\sigma_0 \quad (6)$$

The radial stress component at the delaminated edge, $\sigma_r(R^-)$, depends on the delamination mode of the coating. In the delamination mode schematically shown in Fig. 1 where a substantial annular portion of the delaminated coating remains without buckling as the crack advances, $\sigma_r(R^-)$ is given by [11]

$$\sigma_r(R^-) = -\frac{E_c\varepsilon_\theta(R)[1-(a/R)^2]}{[(1-\nu_c)+(1+\nu_c)(a/R)^2]} \quad (7)$$

where negative denotes compressive.

According to Tresca's yield criterion, the maximum values of the stresses of the coating, σ_r and σ_θ, are limited by the yield stress of the coating, σ_{Yc}, by

$$\sigma_{Yc} \geq |\sigma_r - \sigma_\theta| \quad (8)$$

where σ_θ is the circumferential stress which is given by the generalized Hook's law

$$\sigma_\theta(R) = \frac{E_c}{1-\nu_c^2}[\varepsilon_\theta(R) + \nu\varepsilon_r(R)] \quad (9)$$

and σ_{Yc} is approximately equal to 1/3 of the coating hardness, a well proven relationship valid for majority of engineering materials including ceramics [15].

Therefore, the calculation of the interface toughness requires the determination of the indentation-induced radial and circumferential stains in the coating, ε_{ir} and $\varepsilon_{i\theta}$. For coatings that are very thin compared to the depth of the plastic zone induced by the indentation, the coating has little effect on the deformation of the substrate and it is forced to displace with the surface of the substrate, assuming it remains attached. Thus, when the depth of the indentation-induced plastic zone is much greater than the coating thickness, the essential information needed for determining the indentation-induced radial and circumferential stains in the coating is the radial and circumferential stains of the substrate surface under the indentation.

Calculating the radial and circumferential strains of the substrate surface is rather complicated. However, we can make use of the hemi-spherical cavity model of elastic–plastic indentation [16] to estimate the radial and circumferential stains of the substrate with adequate accuracy. In the model, the contact surface of the indenter is encased in a hemi-spherical 'core' of radius a (Fig. 1). Within the core there is assumed to be a hydrostatic component of stress p. Outside the core it is assumed that the stresses and displacements have radial symmetry and are the same as in an infinite elastic, perfectly-plastic body which contains a spherical cavity under a pressure p. The elastic–plastic boundary lies at a radius c as shown in Fig. 1.

The location of the plastic–elastic boundary, c, is given by [16]

$$c = a\left[\frac{E^* \tan\beta/\sigma_{Ys} + 4(1-2\nu_s)}{6(1-\nu_s)}\right]^{1/3} \quad (10a)$$

where β is the angle of the indenter at the edge of the contact (Fig. 1), σ_{Ys} is the yield stress of the substrate (approximately equal to 1/3 of the substrate hardness), ν_s is the Poisson's ratio of the substrate, and E^* is the contact elastic modulus, defined as

$$\frac{1}{E^*} = \frac{1-\nu_s^2}{E_s} + \frac{1-\nu_i^2}{E_i} \quad (11)$$

where E and ν are Young's modulus and Poisson's ratio of the substrate and the indenter which have subscripts s and i.

When the indenter is a sphere, β is a small angle and, thus, $\tan\beta \approx \sin\beta = a/R_{ind}$, where R_{ind} is the radius of the spherical indenter, and Eq. (10a) becomes

$$c = a\left[\frac{E^* a/(\sigma_{Ys}R_{ind}) + 4(1-2\nu_s)}{6(1-\nu_s)}\right]^{1/3} \quad (10b)$$

According to our early study which has been published elsewhere [17], the radial surface strain is given by

$$\varepsilon_{ir}(R) = -\frac{\sigma_{Ys}}{E^*}\left[6(1-2\nu_s)\ln\frac{c}{R} + \frac{2}{3}(1+\nu_s)\left(\frac{c}{R}\right)^3\right] \quad (12)$$

when the crack front is at the plastic zone ($a \le R \le c$), and

$$\varepsilon_{ir}(R) = -\frac{2}{3}\frac{\sigma_{Ys}}{E^*}(1+\nu_s)\left(\frac{c}{R}\right)^3 \quad (13)$$

when the crack front is at the elastic zone ($c \le R$).

No matter the crack front is at the plastic zone or at the elastic zone, the circumferential surface strain is tensile and is given by [17]

$$\varepsilon_{i\theta} = \frac{\sigma_{Ys}}{3E^*}(1+\nu_s)\left(\frac{c}{R}\right)^3 \quad (14)$$

Therefore, after knowing the Young's modulus, Poisson's ratio and hardness value of each layer of the indented specimen, the thickness and residual stress of the delaminated coating(s), and after measuring the indent radius and the radius of the indentation-induced interface annular crack, the interface toughness can be calculated using Eqs. (2)–(14).

The analysis assumes the interface toughness is governed by the strain energy release rate at the site coincident with the delamination front. With the premise that the surface strain in the substrate is transmitted to the coating as a uniform compression (independent of vertical location in the coating), the interface toughness can be calculated for any multi-layer coating. The result for a multi-layer coating can be derived and reduced to the single-layer solution by represent the multi-layers as a single-layer with an average Young's modulus and an average Poisson's ratio.

3. Measurement procedure

We have developed an experimental procedure for the adhesion measurement. An SOFC with a porous support was measured to demonstrate the use of the indentation method.

3.1. Specimens

Ceremet-supported planar SOFCs with doped ceria electrolytes were developed at the author's group. The SOFCs had excellent powder densities in the operating temperature range of 400–600 °C [3]. Specimens were cut from a half-cell of the cermet-supported SOFCs. The half-cell was fabricated using a conventional wet-processing technology. The processing route of the specimens was: (1) tape-casting a 0.8 mm thick NiO-YSZ (8 mol% Y_2O_3 stabilized ZrO_2) cermet substrate, (2) screen-printing a 15 μm thick NiO-SDC ($(SmO_{1.5})_{0.2}(CeO_2)_{0.8}$) anode layer on the substrate, (3) screen-printing a 15 μm thick SDC electrolyte on the top of the anode layer, (4) sintering the multilayer samples at 1350 °C, and (5) ironing the sintered specimen at 1300 °C. The fabrication details have been described elsewhere [3]. Some of the specimens were made without printing the SDC electrolyte layer in order to obtain one-coating specimens. Fig. 2 shows the polished cross-section of a two-coating specimen of substrate/anode/electrolyte.

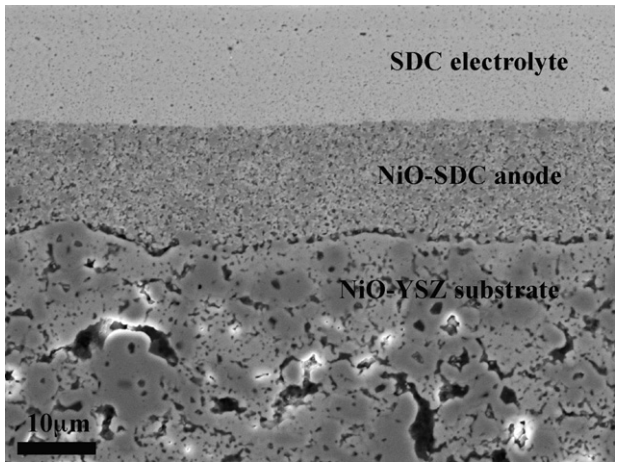

Fig. 2. SEM image of the polished cross-section of the two-coating specimen of substrate/anode/electrolyte.

3.2. Preparation of specimens for indentation testing

Before indentation testing, each specimen was fixed to a thick (>5 mm) metal plate by gluing the back surface of the NiO-YSZ substrate to the metal plate using a adhesive, which had an excellent adhesion strength, because the ceramic specimens were too thin to withstand high load indentation without breaking. In addition to prevent the specimen from breaking in the indentation testing, by using a metal plate with a Young's modulus and a Poisson's ratio close to those of the cermet substrate, the substrate could be regarded as an elastic-plastic half-space; thus the indentation-induced strains could be calculated using Eqs. (10)–(14). The back surface of the NiO-YSZ substrate of each specimen was firstly ground to be flat and smooth, then, the specimen was fixed to the thick metal plate by a cyanoacrylate-based adhesive (the Gripper Super Glue, Super Glue Inc., USA). Only a thin layer of the glue was applied to ensure that the glue could not penetrate into the NiO-YSZ/NiO-SDC interface.

3.3. Indentation testing

Indentation tests were made using a Rockwell C indenter (a spherically tipped conical diamond with a tip radius of 200 μm and an included angle of 120°) and a commercial scratch tester (Revetest, CSEM Instruments SA, Switzerland) after disabling the specimen movement of the tester. Rockwell C indenter is the preferred indenter for the adhesion measurement because it is the most widely used axisymmetric indenter (Rockwell hardness testers and various commercial scratch testers are equipped with Rockwell C indenters) thus readily available. Nevertheless, any hard, spherically tipped indenters (such as the ceramic balls used in Ref. [14]) can be used for the adhesion measurement. To ensure an indenter does not deform plastically during the indentation, the hardness value of the indenter should be at least 1.5 times higher than that of the specimen. The geometry and

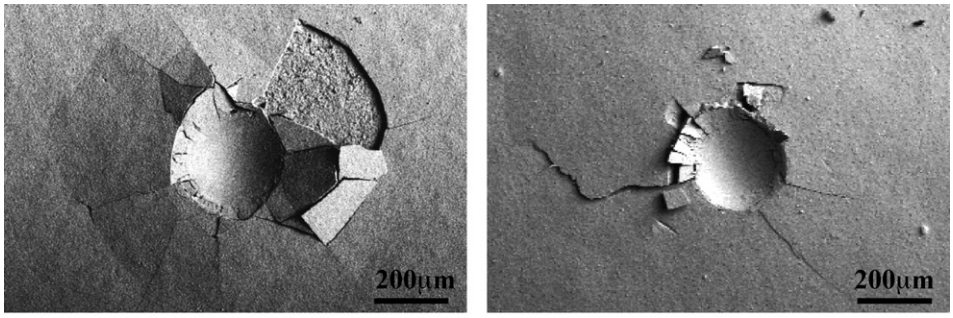

Fig. 3. Top views of indentation delaminations caused by Rockwell C indentaions at 200 N. (a) NiO-SDC coating delaminated from NiO-YSZ substrate and (b) SDC and NiO-SDC coatings delaminated from NiO-YSZ substrate.

elasticity of the indenter have been taken into account in Eq. (10).

According to Section 2, the depth of the indentation-induced plastic zone should be much greater than the coating thickness so that Eqs. (10)–(14) could be used for the determination of the radial and circumferential strains of the coating. On the other hand, the depth of the indentation-induced plastic zone should be constrained within the cermet substrate (not extending into the supporting metal plate because the metal plate had a different plastic property from that of the cermet substrate). An indentation load of 200 N was used in the experiment. This load yielded a depth of plastic zone of 0.288 mm according the following calculation. In each indentation, the indentation load was linearly increased from 0 to 200 N in 60 s.

In each of the indentation test, coating delamination was generated without macrocrack propagating in the NiO-YSZ substrate. Fig. 3(a) shows a typical delamination of the anode layer from the substrate caused by the indentaion. When the indenter was forced through the coating and into the underlying substrate, coating delamination took place with an unbuckled annular plate of coating behind the advancing interface crack front. Simultaneously, tensile hoop stresses developed in the coating surface as the coating was displaced radially during the indentation. The tensile hoop stresses caused radial cracks in the brittle coating. On all of the indented specimens, the radial cracks were not beyond the delamination front. Because the interface toughness is governed by the strain energy release rate at the site coincident with the delamination front, the radial cracks should not have an effect on the calculation of the interface toughness. When the indenter was withdrawn from the coating surface, the elastic component of the indentation-induced deformation in the coating–substrate system was recovered. Due to the difference in elasticity between the coating and the substrate, there was a mismatch of elastic recovery between the delaminated coating and the underlying substrate. The recovery mismatch then caused the buckling of the delaminated coating and possibly partial spallation of the delaminated coating from the substrate. Because of the buckling of the delaminated coating, the delaminated area could be measured using a non-contacting, three-dimensional surface imaging system (WYKO NT-2000, Veeco Instruments Inc., USA). Fig. 4 shows the surface profiles of the indents made on a bare NiO-YSZ specimen and on a one-coating NiO-SDC/NiO-YSZ specimen (the same one as Fig. 3(a)). According to the lift-up profile of the delaminated coating due to the buckling, the diameter of the delamination area was measured.

An examination of the indented specimens revealed that, in the indentations made on the two-coating specimens, all interface delaminations occurred at the anode/substrate interface. None of the delaminations was at the electrolyte/anode interfaces. This indicates that the electrolyte/anode interface had better adhesion than that of the anode/substrate interface. Compared with the single anode layer in the one-coating specimen, the electrolyte and the anode layers in the two-coating specimen had a higher mechanical strength (dense SDC is stronger than porous NiO-SDC) and was thicker. As a result, both the radial tensile cracking and the recovery bucking/spallation were less pronounced on the two-coating specimens, as shown in Fig. 3(b). In addition, the variation of the measured diameter of the delamination area at different circumferential positions on a two-coating specimen was much higher than that on a one-coating specimen. The ratio of the variation to the average diameter of a delamination area was about 80% on a two-coating specimen and about 30% on a one-coating specimen. Because the calculated interface toughness value is very sensitive to the measured radius of the indentation-induced annular crack, only the indentations made on the one-coating specimens were used to calculate the interface toughness. In this experiment, three one-coating specimens were used and three indentations were made on each specimen. Table 1 lists the measured values of the indent diameters and the diameters of delamination areas. The average radius of the delamination area from the nine indentations was used for calculating the interface toughness. The diameter of each indent, which was around 228 μm, was measured using an optical microscope.

3.4. Measurement of mechanical properties

The calculation of the interface toughness using Eqs. (2)–(14) requires using Young's modulus, Poisson's ratio and the hardness value of every layer in a specimen. Poisson's ratio of 0.3 was used for all the NiO-YSZ, NiO-SDC and SDC layers according to the measurements made on similar materials [18]. Young's moduli and hardness values of the three layers were measured on polished surfaces of the layers parallel to the interfaces by

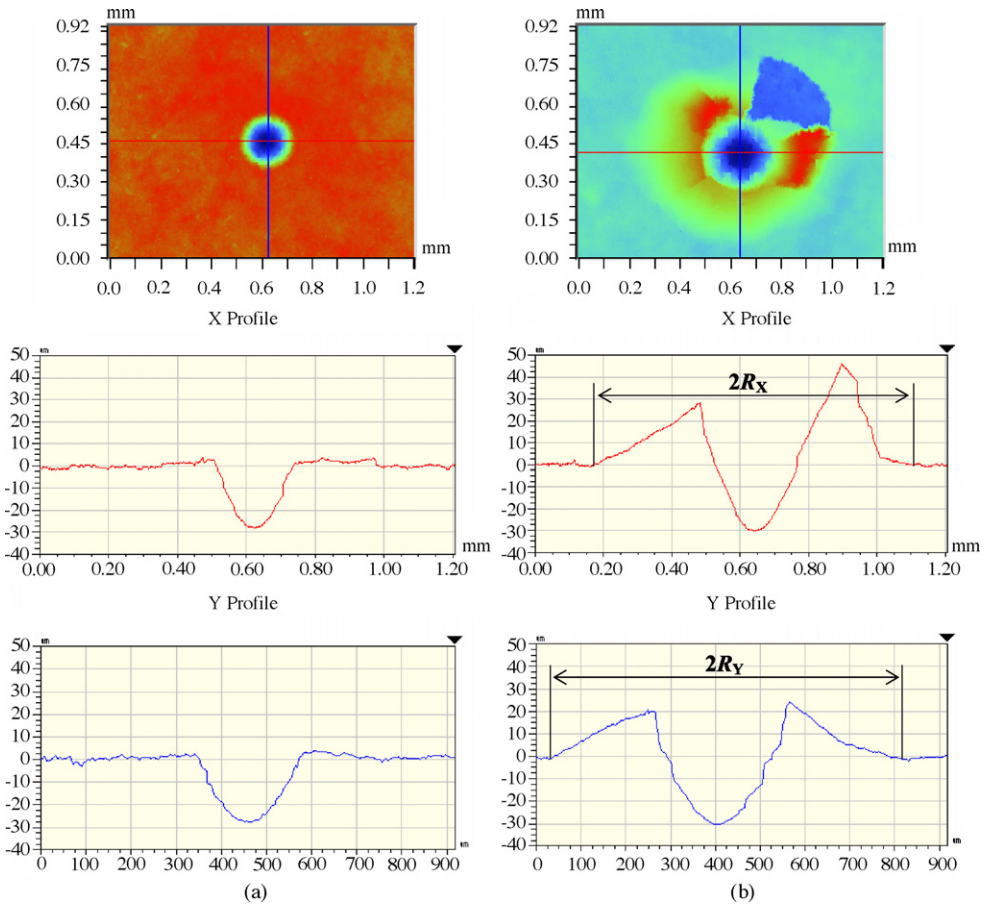

Fig. 4. Profiles of indents made on (a) uncoated NiO-YSZ and (b) one-coating specimen of NiO-SDC on NiO-YSZ substrate.

depth-sensing indentation using a Berkovich diamond indenter at a load of 100 mN (for Young's modulus) and by micro indentation using a Vickers diamond indenter at a load of 2.94 N (for hardness). The measured values are listed in Table 2.

3.5. Measurement of residual stress

Because of the differences in thermal expansion coefficients between the substrate, the anode and the electrolyte layers, the

Table 2
Measured Young's modulus, hardness and residual stress

Layer	Material	Young's modulus, E (GPa)	Hardness, H (GPa)	Residual stress, σ_0 (MPa)
Electrolyte	SDC	208	9.1	+8[a]
Anode	NiO-SDC	168	4.1	+74[a]
Substrate	NiO-YSZ	147	3.7	

[a] Positive denotes tensile.

Table 1
Measured indent diameters and diameters of delamination areas

Specimen	Indentation	Diameter of indent $2a$ (μm)	Diameter of delamination area $2R$ (μm)		
			Measured at X-direction	Measured at Y-direction	Average
	1		934	688	811
1	2		799	636	718
	3		816	636	726
	1		904	786	845
2	2	~228	849	895	872
	3		829	880	855
	1		534	681	608
3	2		783	673	728
	3		708	670	689
Average		228			761

Table 3
Measured values of the interface adhesions

Interface	Material	Interface adhesion	
		Interface toughness, Γ_c (J m^{-2})	Interface fracture toughness, K_{IIC} (MPa m$^{1/2}$)
Anode/substrate	NiO-SDC/NiO-YSZ	1.51	0.51
Electrolyte/anode	SDC/NiO-SDC	>1.51	>0.56

multi-layer specimens were subject to residual stresses after cooling from the ironing temperature of 1300 °C. The residual stresses of the NiO-SDC and SDC layers, which were required for calculating the interface adhesion, were measured using the well-established plate deflection method.

In a specimen of a coating on a substrate, the force contributed by the residual stress in the coating causes the specimen to bend if the substrate is not very thick. The curvature of the specimen caused by the bending depends on the residual stress and thickness of the coating, and the elasticity and thickness of the substrate. The technique of the residual stress measurement comprised: (1) the top SDC surface of a two-coating specimen, or, the top NiO-SDC surface of the one-coating specimen was fixed to a thick (>5 mm) metal plate using a cyanoacrylate-based adhesive. The metal plate prevented the specimen from bending and acted as a specimen holder during the following thinning process; (2) the NiO-YSZ substrate of the specimen was thinned to about 0.25 mm by precision grinding; (3) the radius of curvature of the ground substrate surface was measured using a three-dimensional surface imaging system; (4) the thinned sample was released from the thick metal plate by dissolving the adhesive in acetone, then, the released sample's new radius of curvature measured as before; (5) the difference in curvature before and after releasing the sample, $\Delta\kappa$, was obtained and the average residual stress value in the coating, σ_0, is determined by [19]

$$\sigma_0 = \Delta\kappa \frac{E_s h_s^2}{6h_c(1-\nu_s)} \tag{15}$$

where E_s, h_s and ν_s are the Young's modulus, thickness and Poisson's ratio of the substrate, and h_c is the thickness of the coating. When measuring the average residual stress of the coatings in the two-coating specimen, h_c is the sum of the SDC layer and the NiO-SDC layer. The measured values are given in Table 2.

3.6. Calculation of interface adhesion

The toughness of the anode/substrate interface was then calculated by Eqs. (2)–(14) using the values listed in Tables 1 and 2. When using Eq. (11) to calculate the contact elastic modulus, Young's modulus and Poisson's ratio of diamond, 1141 GPa and 0.07 [20], were used for the indenter. The calculation gave the radius of the elastic–plastic boundary $c = 0.288$ mm, a value less than the radius of the indentation-induced annular crack R (refer to Table 1). Therefore, the front of the indentation-induced annular crack was at the elastic zone. Then, the value of the anode/substrate interface toughness $\Gamma_c = 1.51$ J m^{-2} was determined. As mentioned in Section 3.3, because all of the indentation-induced delaminations occurred at the anode/substrate interface and none of the delaminations was at the electrolyte/anode interfaces, which indicates that the electrolyte/anode interface had better adhesion than that of the anode/substrate interface, the toughness of the electrolyte/anode interface should be greater than 1.51 J m^{-2}.

Since all the indentation-induced delaminations (unbuckled during the indentation, as described in Section 3.3) were due to shearing (mode II) interface cracking only (no contribution from opening mode or tearing mode cracking), the interface fracture toughness, K_{IIC}, can be given by [21]

$$G = \frac{1}{2}(1-\beta^2)\left[\frac{1-\nu_1^2}{E_1} + \frac{1-\nu_2^2}{E_2}\right] K_{IIC}^2 \tag{16}$$

where E and ν are Young's moduli and Poisson's ratios of the two adjacent layers forming the interface which have subscripts 1 and 2, and β is the second Dundurs' parameter defined as

$$\beta = \frac{1}{2}\frac{\mu_1(1-2\nu_2) - \mu_2(1-2\nu_1)}{\mu_1(1-\nu_2) + \mu_2(1-\nu_1)} \tag{17}$$

with $\mu_1 = 0.5E_1/(1+\nu_1)$ and $\mu_2 = 0.5E_2/(1+\nu_2)$.

Using the two equations, the fracture toughness values of the anode/substrate interface and the electrolyte/anode interface were calculated and listed in Table 3.

Because no quantitative adhesion measurement had ever been made on an SOFC according to current publications, no adhesion data are available for comparison against the interface adhesion measured in this study. An interface between two brittle layers usually has a toughness value of less than 5 J m^{-2} [22]. Considering that the porous microstructures of the NiO-YSZ substrate and the NiO-SDC layer presented many flaws at the NiO-SDC/NiO-YSZ interface which facilitated the development of interface cracking, the measured value of the interface toughness is reasonable. Fuel cell testing showed that there was no significant drop in the power output from such a cell after 12 thermal cycles. The fuel cell testing result demonstrated that the SDC/NiO-SDC and NiO-SDC/NiO-YSZ interfaces had sufficient adhesion to ensure good fuel cell performance during operation.

4. Discussion

In this study, high load indentation using a spherically tipped indenter was used to measure the interface adhesion of a cermet-supported, co-sintered substrate-anode-electrolyte half-cell. The same procedure can also be used for measuring the adhesion of

the cathode-electrolyte interface of the cermet-supported SOFC. This method should also be suitable for the adhesion measurements of other SOFCs as long as propagating macrocracks do not develop at the substrate to rupture the specimen during the indentation. The method is ideal for a metal-supported SOFC where the ductile metallic substrate can withstand severe plastic deformation without rupture. The method can also be used for the adhesion measurement of an anode or cathode-supported SOFC in terms of a similar porous microstructure to the cermet substrate used in this study.

The indentation method, however, might not be applicable to an electrolyte-supported SOFC because an SOFC electrolyte, which is a brittle ceramic with a dense and uniform microstructure, is very likely to rupture in the high load indentation. When a dense and uniform ceramic is indented by a hard, spherically tipped indenter at a high load, Hertzian cone fracture is very likely to occur in the specimen. The Hertzian cone fracture begins as a surface ring crack outside the elastic contact and then, at a higher load, propagates downward and flares outward within a modest tensile field into a stable, truncated cone configuration [23]. Therefore, although the high load indentation method is suitable for any SOFC with a porous support, it might not be applicable to an electrolyte-supported SOFC.

5. Conclusions

Various methods for measuring the adhesion of a ceramic coating to the underlying substrate were reviewed. Among them, high load indentation using a hard, spherically tipped indenter is the most appropriate method for the adhesion measurements of SOFCs. This method should be suitable for the adhesion measurement of any SOFC with a porous support. A measurement procedure and the related calculation equations have been developed. The measurement made on a cermet-supported SOFC with a doped ceria electrolyte indicated that the minimum interface toughness and minimum interface fracture toughness of the cell were 1.51 J m^{-2} and 0.51 MPa $m^{1/2}$.

References

[1] F. Tietz, H.-P. Buchkremer, D. Stöver, Solid State Ionics 152–153 (2002) 373–381.
[2] N.P. Brandon, A. Blake, D. Corcoran, D. Cumming, A. Duckett, K. El-Khoury, D. Haigh, C. Kidd, R. Leah, G. Lewis, C. Matthews, N. Maynard, N. Oishi, T. McColm, R. Trezona, A. Selcuk, M. Schmid, L. Verdugo, J. Fuel Cell Sci. Technol. 1 (2004) 61–65.
[3] X. Zhang, M. Robertson, C. Decès-Petit, Y. Xie, R. Hui, S. Yick, M. Staite, E. Styles, J. Roller, R. Maric, D. Ghosh, in: S.C. Singhal, J. Mizusaki (Eds.), Solid Oxide Fuel Cells IX (SOFC-IX), The Electrochemical Society, Inc., 2005, pp. 1102–1109.
[4] O.A. Marina, C. Bagger, S. Primdahl, M. Mogensen, Solid State Ionics 123 (1999) 199–208.
[5] ASTM C633-01, Annual Book of ASTM Standard, vol. 03.01, ASTM International, West Conshohocken, PA, USA, 2001.
[6] 3M Engineering Adhesion Division, Technical Data of 3M Scotch-Weld™ Epoxy Adhesives, 3M, St. Paul, USA, 2002.
[7] P.G. Charalambides, J. Lund, A.G. Evens, R.M. McMeeking, J. Appl. Mech. 56 (1989) 77–82.
[8] I. Hofinger, M. Oechsner, H.-A. Bahr, M.V. Swain, Int. J. Fracture 92 (1998) 213–220.
[9] Y. Xie, H.M. Hawthorne, Surf. Coat. Technol. 155 (2002) 121–129.
[10] J. Malzbender, J.M.J. den Toonder, A.R. Balkenende, G. de With, Mater. Sci. Eng. R 36 (2002) 47–103.
[11] M.D. Drory, J.W. Hutchinson, Proc. R. Soc. Lond. A 452 (1996) 2319–2341.
[12] J.J. Vlassak, M.D. Drory, W.D. Nix, J. Mater. Res. 12 (1997) 1900–1910.
[13] Y. Xie, H.M. Hawthorne, Surf. Coat. Technol. 172 (2003) 42–50.
[14] B.R. Lawn, N.P. Paditure, H. Cai, F. Guiberteau, Science 263 (1994) 1114–1116.
[15] A.J. Bushby, M.V. Swain, in: R.C. Bradt, C.A. Brooks, J.L. Roubort (Eds.), Plastic Deformation of Ceramics, Plenum Press, New York, 1995, pp. 161–172.
[16] K.L. Johnson, Contact Mechanics, Cambridge University Press, 1985, pp. 173–175.
[17] Y. Xie, H.M. Hawthorne, Surf. Coat. Technol. 141 (2001) 15–25.
[18] A. Selcuk, A. Atkinson, J. Eur. Ceram. Soc. 17 (1997) 1523–1532.
[19] A.G. Evans, J.W. Hutchinson, Acta Metall. Mater. 43 (1995) 2507–2530.
[20] W.C. Oliver, G.M. Pharr, J. Mater. Res. 7 (1992) 1564–1583.
[21] V. Tvergaard, J.W. Hutchinson, J. Mech. Phys. Solids 41 (1993) 1119–1135.
[22] A.G. Evans, J.W. Hutchinson, Y. Wei, Acta Mater. 47 (1999) 4093–4113.
[23] B.R. Lawn, J. Am. Ceram. Soc. 81 (1998) 1977–1993.